Available online at www.sciencedirect.com
SCIENCE DIRECT®
Journal of Power Sources 136 (2004) 122–131
JOURNAL OF POWER SOURCES
www.elsevier.com/locate/jpowsour

Effect of silver co-sputtering on amorphous V_2O_5 thin-films for microbatteries

Jae Myung Lee [a], Ho-Sung Hwang [b], Won-Il Cho [b], Byung-Won Cho [b], Kyoo Young Kim [a,*]

[a] *Department of Materials Science and Engineering, Center for Advanced Aerospace, Pohang University of Science and Technology, San 31, Hyoja-dong, Pohang, Kyung-buk 790-784, South Korea*

[b] *Environment and Process Technology Division, Korea Institute of Science and Technology, 39-1, Hawolgok-dong, Seongbuk-gu, Seoul 136-791, South Korea*

Received 2 February 2004; accepted 17 May 2004

Available online 3 August 2004

Abstract

The effect of silver co-sputtering on the microstructural and electrical properties of amorphous V_2O_5 films is investigated. The films are grown by dc reactive sputtering and are applicable to thin-film microbattery cathodes. Analysis with glancing-angle X-ray diffraction (GXRD), scanning electron microscopy (SEM), X-ray photon spectroscopy (XPS), and Fourier transformation infrared (FT-IR) spectroscopy confirm that the growing rate, silver content and microsturucture of the V_2O_5 films are dominantly affected by the r.f. power supplied on the silver metal targets. The discharge capacity and cycle ability of microbatteries increases with increasing silver content in the thin cathode films. In addition, it is found that silver co-sputtered V_2O_5 cathode films, if only obtained at not more than 30 W, exhibit better discharge capacity, cycle ability and lithium-ion diffusivity than an undoped V_2O_5 cathode film. This is due to increases both in the electronic conductivity with doping elements of high electronic conductivity and in the distance between two adjacent V_2O_5 layers by co-sputtered silver atoms.

Keywords: Vanadium pentoxide; Silver co-sputtering; Amorphous film; Microbatteries

1. Introduction

Due to the development of microelectromechanical system (MEMS) technology for microdevices and -sensors, the need for microsize sources is greatly increasing. Two power options that have been considered are energy-storage devices (e.g., batteries and capacitors) and energy-conversion devices (e.g., solar cells, piezoelectric generators) [1]. Among these, thin-film microbatteries offer great promise due to their unique manufacturing advantages, i.e., they can be incorporated into the same integrated circuits as other electronic device elements, and can be used in applications such as smart cards, on-chip power sources and portable electronic devices [2,3].

Practical, rechargeable, thin-film battery systems (lithium metal anode-LiPON electrolyte-transition metal oxide cathode) have been developed by ORNL and are based on thin-film deposition technology of oxides and nitrides [2,3]. Of the numerous cathode materials ($LiCoO_2$, $LiMn_2O_4$, $LiNiO_2$, $LiFePO_4$, etc.) for lithium/lithium-ion thin-film batteries, V_2O_5 is the most promising materials due to its high capacity, cycle stability and ease of preparation. In particular, conventional annealing processes that cause cracking and buckling of thin-films [4] are not required for amorphous V_2O_5 films. The latter films are therefore considered to be the best candidate material for cathodes for on-chipped, thin-film microbatteries [5].

To improve the electrochemical properties of V_2O_5, several researchers have employed alloying or doping processes during materials synthesis. Smyrl and co-workers [6–9] reported that cyclic capacity and cyclic life increased with the addition of doping elements (Ag and Cu) due to increases in cathode material conductivity and reversible local structure modification during charge–discharge cycles. The electrical conductivity of the doped materials was up to three orders of magnitude higher than that of undoped material and there was a concurrent dramatic enhancement in the Li^+ ion diffusion coefficient. These materials were synthesized by the sol–gel method that is not suitable for fabrication processes of thin-film batteries and semiconductor devices. Therefore,

* Corresponding author. Tel.: +82-54-2792134; fax: +82-562-2794499.
E-mail address: kykim@postech.ac.kr (K.Y. Kim).

0378-7753/$ – see front matter © 2004 Elsevier B.V. All rights reserved.
doi:10.1016/j.jpowsour.2004.05.051

it is imperative to develop a suitable doping or co-sputtering process that can be applied to thin-film battery fabrication. Although some research groups [10–12] have studied doping or alloying effects on V_2O_5 films, most have focused on the electrochemical properties of such films. In order to grow amorphous V_2O_5 thin-films, it is very important to obtain a better understanding of the structure and characteristics of co-sputtered cathode films.

This study examines the effect of silver co-sputtering on the electrochemical, structural, chemical and surface properties of amorphous V_2O_5 films deposited by dc reactive magnetron sputtering. The silver content is adjusted by the r.f. power level of co-sputtering on the silver metal target. The film structure is characterized with GXRD, AFM, and SEM; the chemical properties of the films are analyzed by means of FT-IR, XPS and ICP; the electrochemical properties are measured by potentiostatic intermittent titration technique (PITT) and charge–discharge testing.

2. Experimental

Film deposition was carried out in a turbo-pumped chamber with a initial pressure of 8×10^{-6} mbar. Thin films of vanadium oxide were deposited using dc magnetron sputtering of mixed gas (70 vol. % Ar and 30 vol.% O_2) on a vanadium metal target. The flow rates of argon (99.998% purity) and oxygen (99.998% purity) gas were controlled by MFC units (MKS Type-1179A), which were attached to the front of gas inlets, and the pressure of the gas mixture was controlled at 1.33×10^{-2} mbar, by a throttle valve that controlled the conductance of gas flow from chamber to pumping units. A detailed illustration of this sputtering system is given in Fig. 1.

Silver vanadium oxide films were deposited by means of a co-sputtering process, i.e., simultaneous dc magnetron sputtering on the vanadium target (99.9% Cerac). The silver content in the thin-film sample was controlled by an r.f. power level imposed on the silver target with sputtering at a 500 mA dc current on the vanadium metal target. The r.f. power level was set at 0, 10 20, 30 and 40 W, and specimen identification was denoted as VO, A10, A20, A30 and A40, respectively. The target dimensions were: 10.16 cm diameter $\times$ 0.635 cm thickness. The distance between the target and substrate was 10 cm. During the deposition process, the substrate rotated at 10 rpm in order to give uniform deposition of the thin-film.

Film crystallinity was characterized by GXRD and film surface morphology was observed by SEM and AFM. Most GXRD scans used a thin-film attachment and a fixed angle

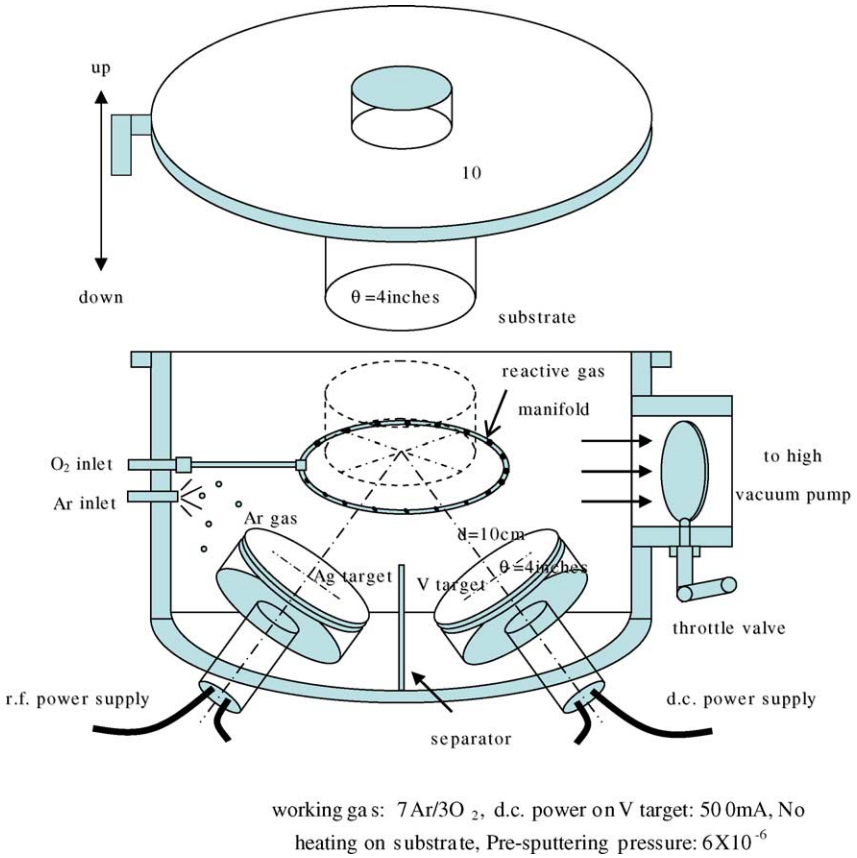

Fig. 1. Schematic illustration of sputtering system. Direct current power is applied to a vanadium metal target and alternative current power is applied to a silver metal target. Details of deposition conditions are also given.

of incidence in order to minimize substrate peak intensities. The vanadium:oxygen (V:O) atomic ratios of the films were analyzed by inductively coupled plasma atomic spectroscopy (ICP) and energy dispersive X-ray analysis (EDX) which was attached to the SEM unit. The properties of the chemical bonding were identified by FT-IR and XPS.

To evaluate electrochemical properties, all-solid-state thin-film battery cells were fabricated on Pt-coated plates. The electrolyte was a 1.4–1.5 μm thick film of lithium phosphorous oxi-nitride (LiPON), which was deposited by r.f. magnetron sputtering of N_2 reactive gas on Li_3PO_4 target [2–4]. The anodes were composed of 2.5–3 μm thick films of lithium metal that were grown by means of thermal evaporation. To obtain film uniformity, the evaporation rate was maintained constant at 4–5 nm s^{-1} by adjusting the power level supplied on the crucible.

3. Results

3.1. Characterization of silver co-sputtered V_2O_5 thin-films

The crystallinity of the silver co-sputtered V_2O_5 and that of the undoped thin-film was characterized by GXRD, as shown in Fig. 2. Various power levels were supplied on the silver target, but there is no crystalline vanadium oxide peak. Only a broad hump is observed around $2\Theta = 13^\circ$, which is common in amorphous V_2O_5 thin-films. A sharp and strong peak around $2\Theta = 40^\circ$ is due to a platinum (1 1 1) layer between the vanadium oxide layer and the glass substrate. The platinum thin-film served as the current-collector in the thin-film battery cathode.

Table 1
Growth rate measured in silver-doped V_2O_5 films

Specimen	R.f. power on Ag (W)	Growth rate (nm min^{-1})
VO	0	1.94
A10	10	1.15
A20	20	1.00
A30	30	1.65
A40	40	4.06

Under low-power conditions, the growth rate decreases on increasing the co-sputtering power level, but increases under high power-conditions.

The thin-film growth rate is not consistent with increasing silver co-sputtering power from 0 to 40 W, as shown in Table 1. In samples VO, A10 and A20, it decreases as the power supplied on the silver target is increased. The growth rate of A10 is 1.15 nm per min, and that of A20 is 1.00 nm per min, which is half of the undoped sample's growth rate (1.94 nm per min), but the growth rate increases as the power level increases over 30 W as shown in sample A30 (1.65 nm per min) and A40 (4.06 nm per min).

Thin-film chemical compositions were determined by ICP analysis as shown in Fig. 3. As the oxygen composition gave a variety compounds, viz., $Ag_xV_2O_{4.9}$ to $Ag_xV_2O_{5.2}$, the oxygen stoichiometry was set at 5 for convenience. The composition of the thin-film was V_2O_5, $Ag_{0.1}V_2O_5$, $Ag_{0.3}V_2O_5$, $Ag_{0.8}V_2O_5$, and $Ag_{1.8}V_2O_5$ for samples VO, A15, A20, A30 and A40, respectively.

The AES depth profiles for the thin-films are shown in Fig. 4. All samples were sputter-etched at the rate of 40 nm per min argon plasma until a platinum peak, which acted as a current-collector layer, was detected. The atomic fraction of oxygen was highest at the cathode surface because an air-formed oxide layer was grown on the surface during sample handling. The distribution of oxygen and vanadium

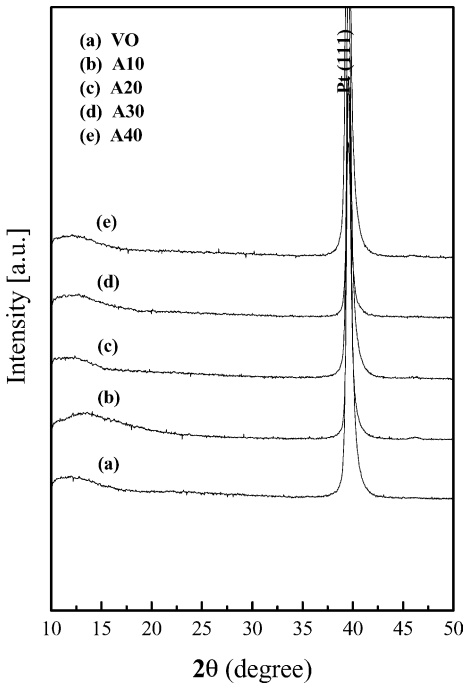

Fig. 2. Glancing angle X-ray diffraction patterns of a V_2O_5 film and silver-doped V_2O_5 films that shows non-crystallinity of thin-films.

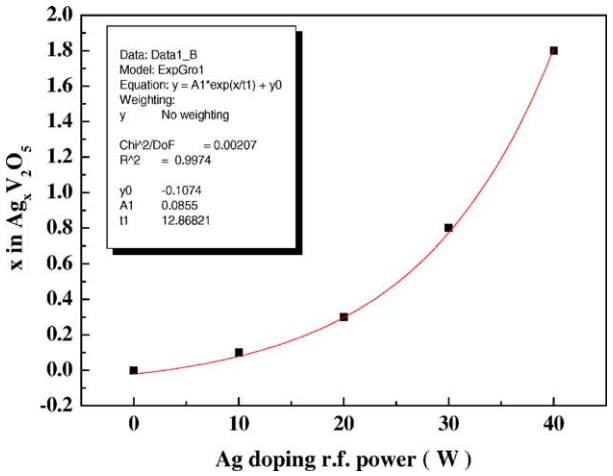

Fig. 3. Silver content in thin-films measured by ICP analysis. Silver content (log scale) vs. co-sputtered power level.

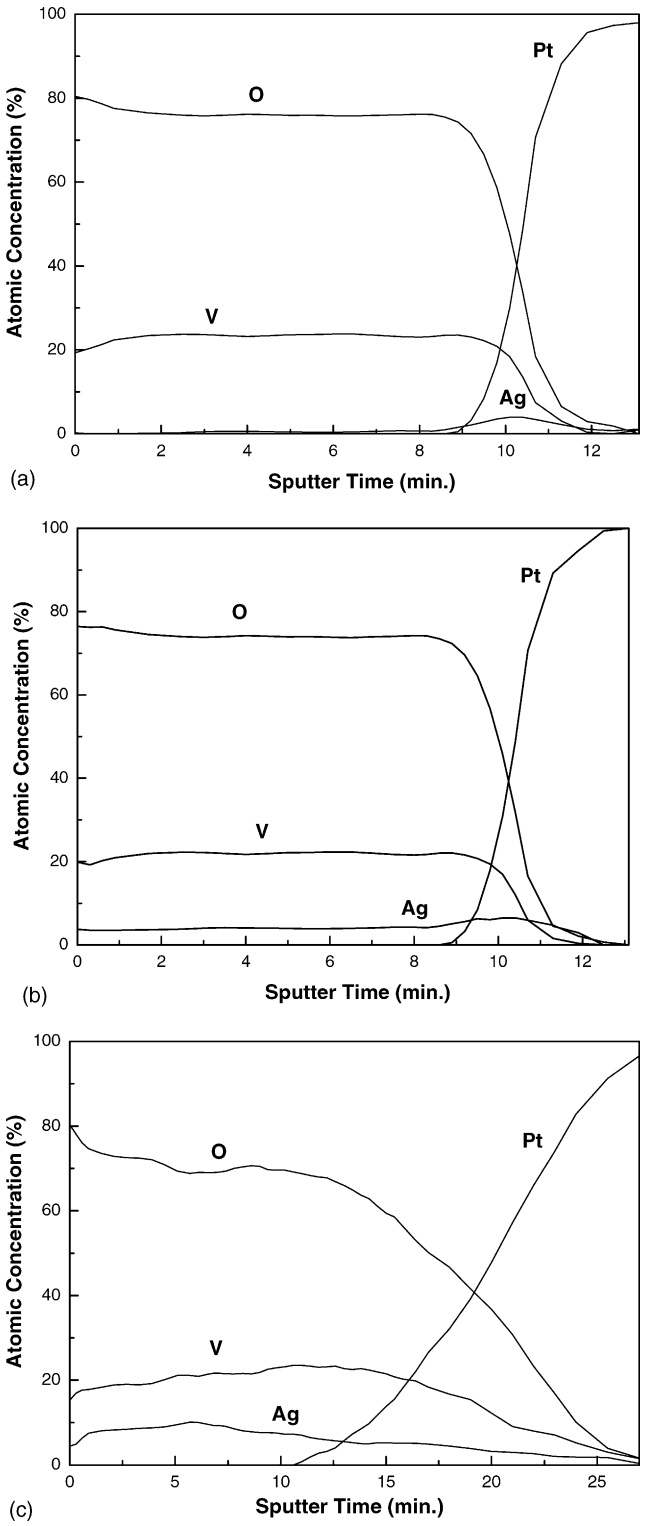

Fig. 4. AES depth profile of Ag-doped V_2O_5 films: (a) A20, (b) A30, and (c) A40. (Samples etched by argon plasma at 40 nm per min.)

is consistent through the thickness beneath the air-formed oxide layer. The silver content in the film increases with increase in the silver co-sputtered level as expected. Nevertheless, the distribution of silver through the film is not uniform in all samples. There is a silver concentrated layer (4 at.%), which appears as a hump between the platinum current-collector and the silver-doped vanadium oxide thin-film. The total content in the sample is reduced close to the top surface. The thickness of the silver concentrated layer also increases as the silver co-sputtered power is increased, i.e., 120 nm for sample A10 and 160 nm for sample A30.

The chemical distribution of sample A40 is quite different from that of the other sample. The distribution of all elements is not constant through the film. There is a silver concentration hump (10 at.%) near the top surface and the silver concentration decreases with increasing film thickness. The concentration of silver at the interface between the platinum current-collector layer and vanadium oxide layer is lower than in other regions (5 at.%).

3.2. Electrochemical test of Ag co-sputtered V_2O_5 thin-films

To investigate electrochemical properties, a solid-state thin-film battery was fabricated with the configuration of: Li (anode)/LiPON/Ag-V_2O_5/(Pt) (current collector), as shown in Fig. 5.

The specific capacity of the battery is shown in Fig. 6 when charged and discharged for 200 cycles between 3.6 and 1.5 V at a constant current density of 20 μAh cm^{-2} μm. It is clearly seen that cells with silver-doped vanadium oxide cathodes exhibit better capacity and cyclic ability, except the cell with A40, compared with that of undoped V_2O_5. For the undoped sample, the discharge capacity is 53 μAh cm^{-2} μm during the first cycle, but increases sharply to 65 μAh cm^{-2} μm during the second cycle. With further cycling it decays slowly with increasing cycle number to 55 μAh cm^{-2} μm after 200 cycles. The discharge capacity of thin-film battery cells with A10 and A20 also decays with cycle number, but the capacity during the initial cycle is higher than that for the undoped sample. For cells with A10 whose capacity is 77 μAh cm^{-2} μm during the first cycle, it decays to 67 μAh cm^{-2} μm after 20 cycles. By contrast, for cells with A20, the capacity decays from 74 μAh cm^{-2} μm during the first cycle to 66 μAh cm^{-2} μm after 200 cycles. The initial cell capacity of cells with sample A30 (78 μAh cm^{-2} μm) is similar to that of other silver-doped cells, but it maintains its initial value for more than 200 cycles (73.6 μAh cm^{-2} μm). The discharge capacity of A40 cells is different from other doped cells. Not only is the initial value lower than those of the others, but also it decays rapidly with increasing cycle number.

Lithium-ion diffusivity into the cathode thin-film was measured by PITT, as shown in Fig. 7. The voltage of the thin-film battery was controlled from 3.5 V down to 1.5 V with series of voltage steps. Each step was 200 mV and the time to reach the current equilibrium was 1200 s. According to the results, the diffusivity of lithium ions into sample 30A is about 10 times higher than that of the others.

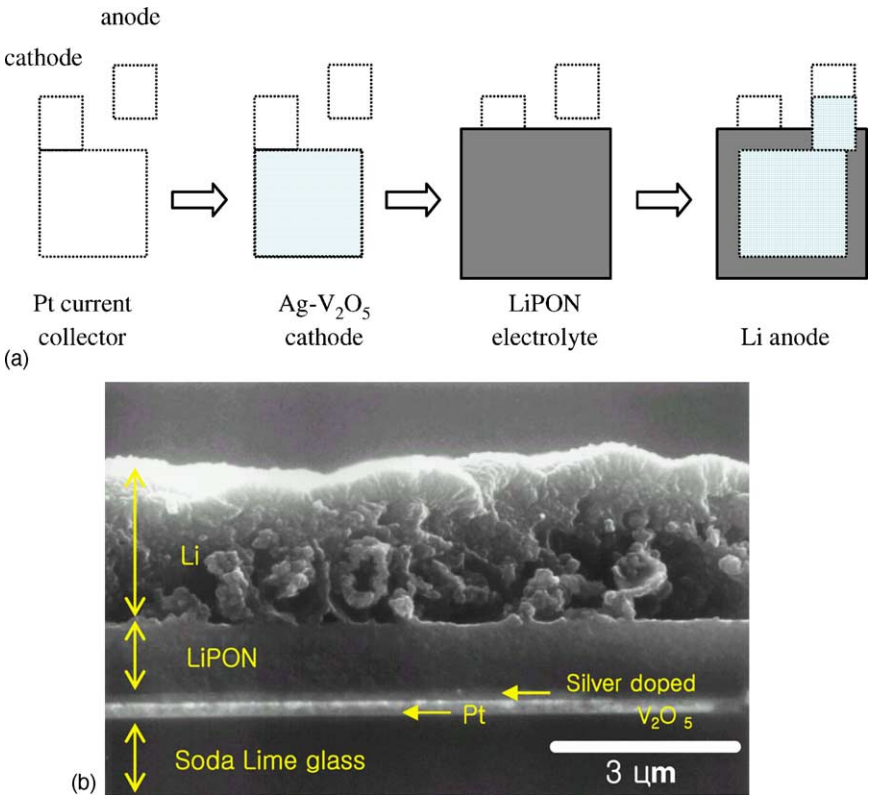

Fig. 5. (a) Thin-film microbattery fabricated with configuration: Li/LiPON/Ag-V_2O_5/Pt on soda lime glass, (b) cross-sectional view of thin-film microbattery.

3.3. FT-IR and XPS analysis

The FT-IR absorption bands for V_2O_5 films deposited with increasing silver r.f. power are shown in Fig. 8. All samples show broadened absorption bands that are characteristic of a random structure with a wide distribution of V–O bond length and angle. By comparison with a r.f. sputtered polycrystalline V_2O_5 thin-film [13] (V=O bonds stretching: 1020 cm^{-1}, V–O–V bonds vibration: 840, 433 cm^{-1}, and $V-O\lessgtr^{V}_{V}$ bonds vibration: 535–525 cm^{-1}),

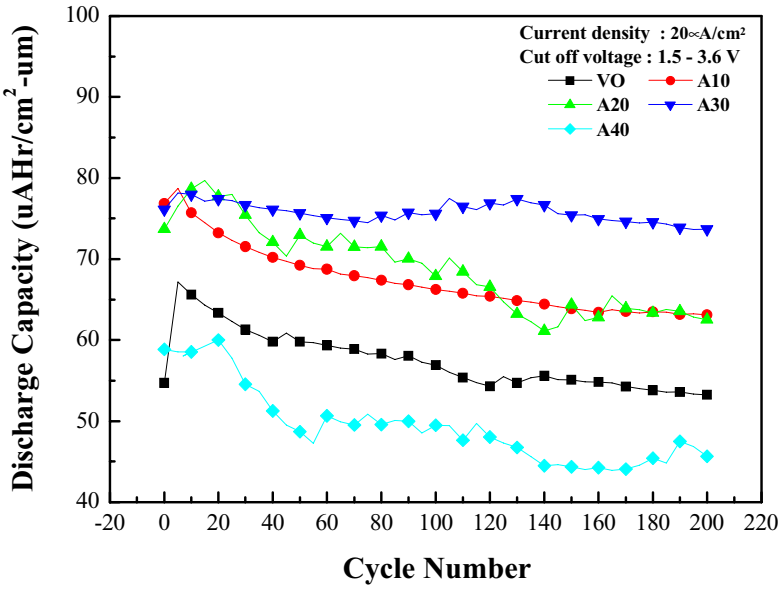

Fig. 6. Discharge capacities of thin-film batteries made from amorphous V_2O_5 films with different contents of silver (cycled between 3.6 and 1.5 V) as function of cycle number.

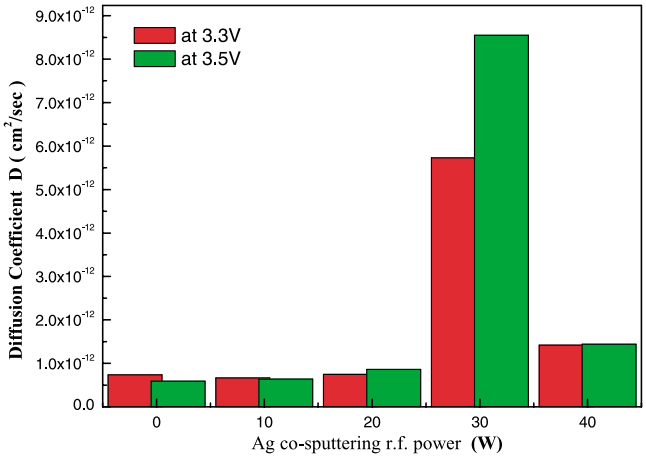

Fig. 7. Lithium-ion diffusivity in Ag co-sputtered V_2O_5 thin-film measured by PITT (potentiostatic intermittent titration technique) from 3.5 to 1.5 V with series of 200 mV voltage steps.

broadened peaks, which indicate a double bond V=O vibration around 970–1020 cm^{-1} and V–O–V vibration around 820 and 580 cm^{-1}, remain in the amorphous state. There are many small unidentifiable around 450–570 cm^{-1}.

On increasing the silver co-sputtering power, a strong absorption peak around 1020 cm^{-1} in undoped sample shifts to lower wave number (1005 → 995 → 970 → 940 cm^{-1}) and the A40 spectrum is different from that of others. These two facts are thought to be closely related to structural changes in the thin-film during the deposition process on increasing silver co-sputtering power level.

XPS measurements were performed on samples A40 and A30, as shown in Fig. 9. The relative peak intensities of atomic core level spectra in A30 are different from those of A40. In the core level of V 2p and O 1s atoms, the peak intensity of A30 is 1.5 times larger than that of A40 as shown in Fig. 9(a). On the other hand, the peak intensity of the Ag 3d level in A40 is three times larger than that of A30 as shown in Fig. 9(b), which indicates a greater amount of silver in A40 compared with A30. In A30, the V $2p^{3/2}$ core level binding energy is 517.05 eV, with a chemical shift of $\Delta E = +4.65$ eV (metallic V $2p^{3/2}$ core level = 512.4 eV), and the spin orbit splitting between the V $2p^{3/2}$ and the V $2p^{3/2}$ peaks is 7.5 eV. The core level binding energy of A30 is in good agreement with that reported by other workers [14,15]. The V $2p^{3/2}$ core level binding energy of A40 shifts to 516.05 eV (chemical shift $\Delta E = +3.65$ eV), which indicates a loss of positive charge in the vanadium core.

The silver core level binding energy of A30 Si the same as that of A40 (Ag $3d^{5/2}$ = 367.35 eV, Ag $3d^{5/2}$ = 373.35 eV, and spin orbit splitting = 6 eV), which shifts to a lower value compared with that of metallic silver (Ag $3d^{5/2}$ = 368.3 eV) [13].

The oxygen core level spectra O 1s were de-convoluted as shown in Fig. 9(c) for A30 and Fig. 9(d) for A40. Both spectra were de-convoluted in three peaks (529.89, 531.30 and 532.29 eV in A30 and 529.63, 530.95 and 532.21 eV in A40). The first peak is related to the presence of silver oxides (Ag_2O, AgO = 528.6–530 eV [14]), the second peak is related to the presence of vanadium oxides (V_2O_5, V_2O_4, V_2O_3, V_2O = 529.8–530.4 eV [15]), and the third peak is related to contaminant water (H_2O = 532.8–533.2 eV [13]). The intensity of the first peak in A30 is 1.5 times larger than that of A40, which suggests differences in ionic state of silver.

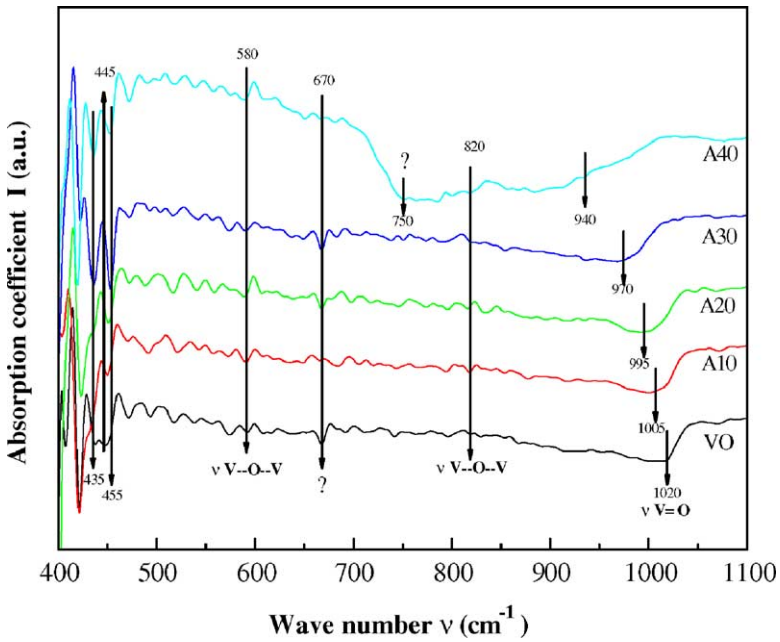

Fig. 8. FT-IR absorption spectra of silver-doped V_2O_5 thin-film samples. Vynyl V=O bond shifts to lower wave number with increase in silver co-sputtering power level (VO = amorphous V_2O_5; A10 = 10 W; A20 = 20 W; A30 = 30 W; A40 = 40 W).

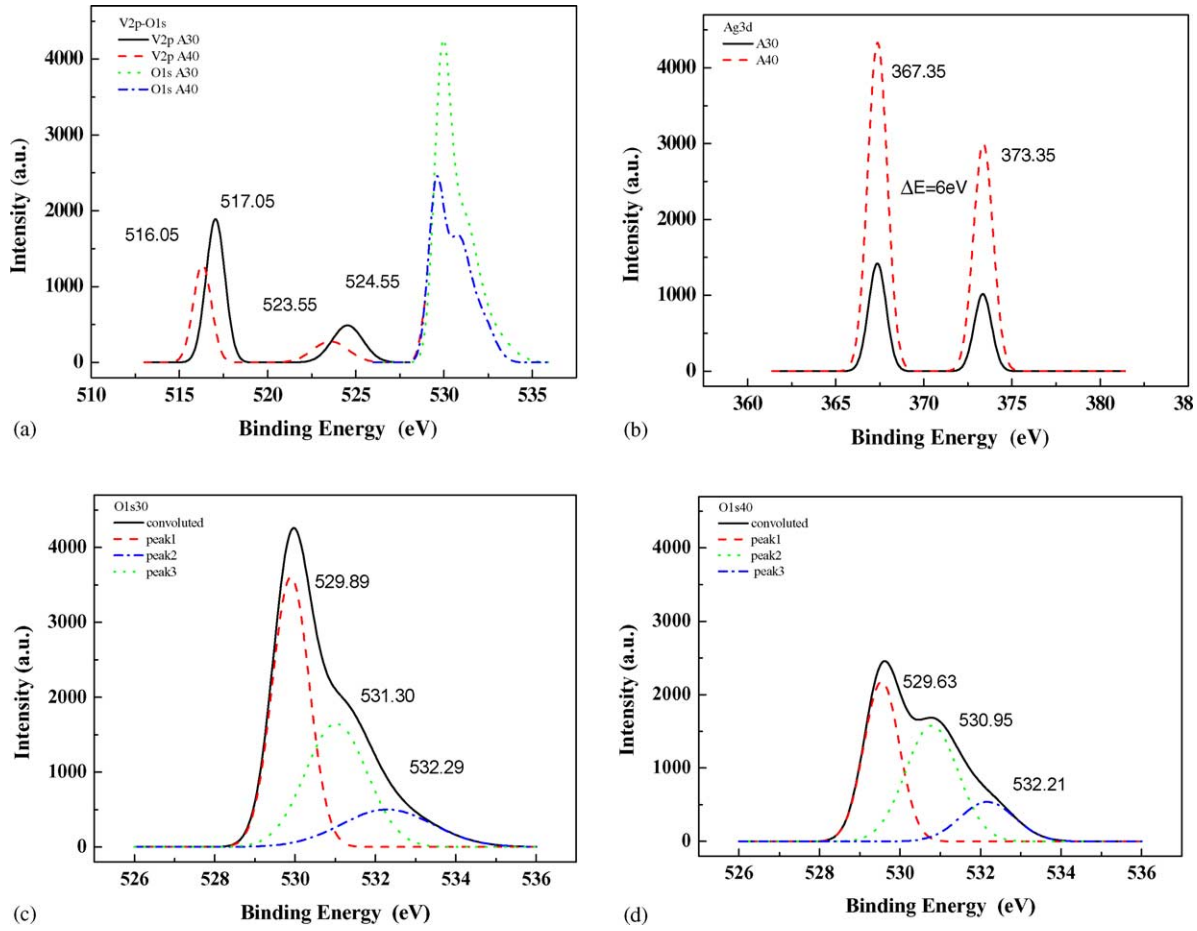

Fig. 9. X-ray photon spectra for samples A30 and A40: (a) core level of V and O atom, (b) 3D-level of Ag, (c) convoluted curves of O 1s level of A30, and (d) convoluted curves of O 1s level of A40.

3.4. Surface analysis

Surface morphology changes due to increasing silver co-sputtering power were examined by SEM and AFM analysis. Some selective SEM images of silver co-sputtered thin-films on a Pt/glass substrate are presented in Fig. 10. On increasing silver co-sputtering power, the grain size of the thin-films increases as shown in surface images (Fig. 9(a-c)). In these images, all samples are seen to consist of clusters of 2–3 grains. The grains in sample VO are as small as 1–10 nm, while grains in the other samples are about 10–50 nm. All samples, except A40, consist of closely packed, long, columnar grains which grow from the platinum current-collector surface towards the outside, as shown in the cross-sectional image. The diameter of these columns is of the same size as the cluster and consist of 2–3 grains. The cross-sectional view of A40 is different from the others. Sample A40 consist of clusters of oxide which look like lumps of wheat dough with a high quantity of voids as shown in Fig. 10(f).

The surface roughness of the samples was measured by AFM. The surface roughness of A40 is about six times larger than that of VO, as shown in Fig. 11. The surface roughnesses of VO and those of the silver-doped samples, except A40, are similar.

4. Discussion

The effect of silver co-sputtering on the growth of amorphous V_2O_5 thin-film is complicated. The silver content in the thin-film increases exponentially on increasing the co-sputtering power level but the growth rate and silver distribution are not coincident with the silver co-sputtering power level. The growth rate decrease on increasing co-sputter power to <30 W, otherwise it increases, and the silver content in the thin-film is not constant through its thickness. Silver is not distributed well in the thin-films, but accumulates at the interface of the platinum current-collector and the amorphous V_2O_5 layer except in the 40 W co-sputtered thin-film. These phenomena can be explained by the sputter yield amplification (SYA) mechanism [16] as follows.

4.1. Selective sputtering of multi-atom flux condition

During the sputtering collision process, heavier atoms penetrate deeply and so they usually adhere to the substrate better than lighter atoms even if they erode the substrate surface more than lighter atoms do. In the case of multi-atom

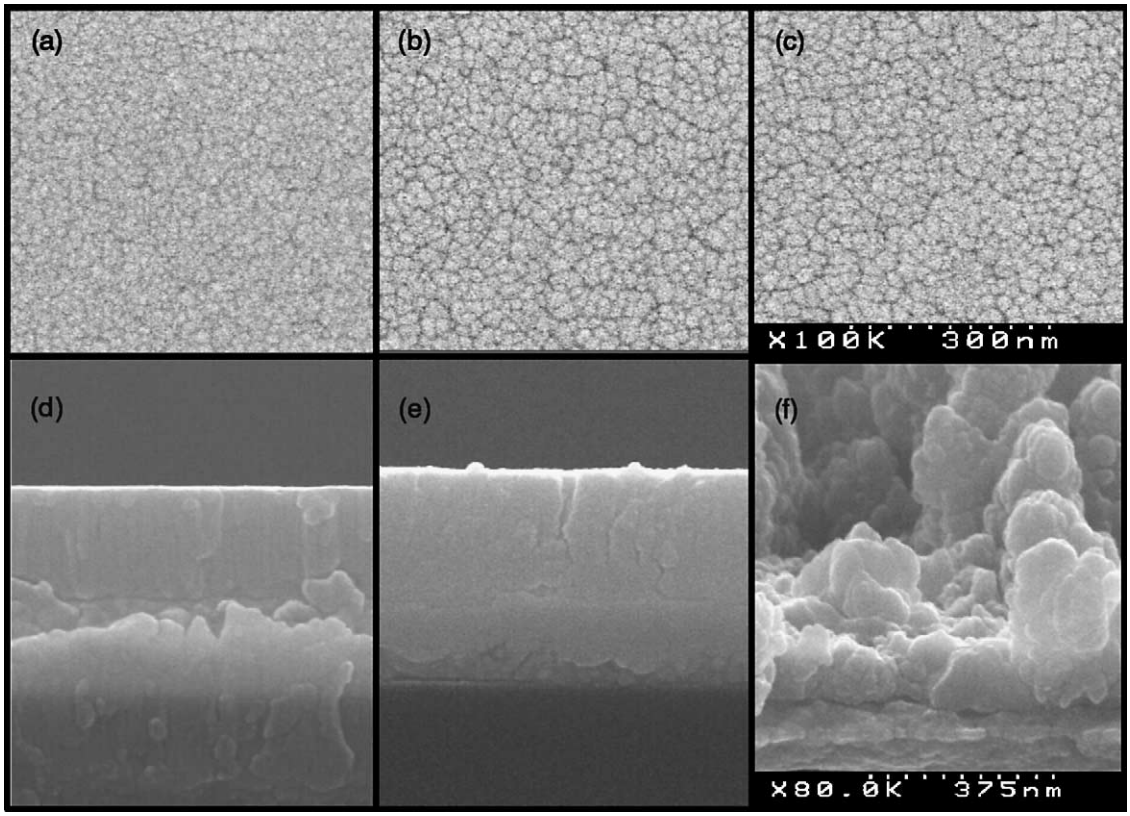

Fig. 10. SEM images of V_2O_5 sample and Ag 40 W co-sputtered V_2O_5 sample: (a–c) are surface images of VO, A30 and A40 (magnification of 100 000×), (d–f) are cross-sectional images of VO, A30 and A40 (magnification of 80 000×).

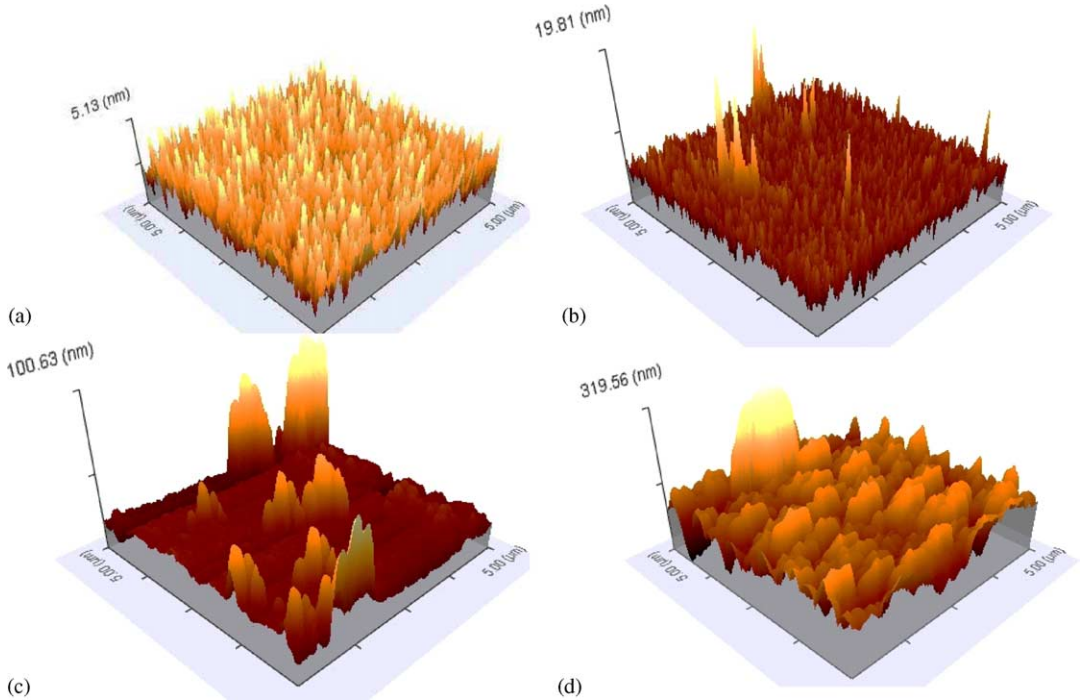

Fig. 11. AFM mages of sample surface: (a) VO, (b) A10, (c) A30, and (d) A40.

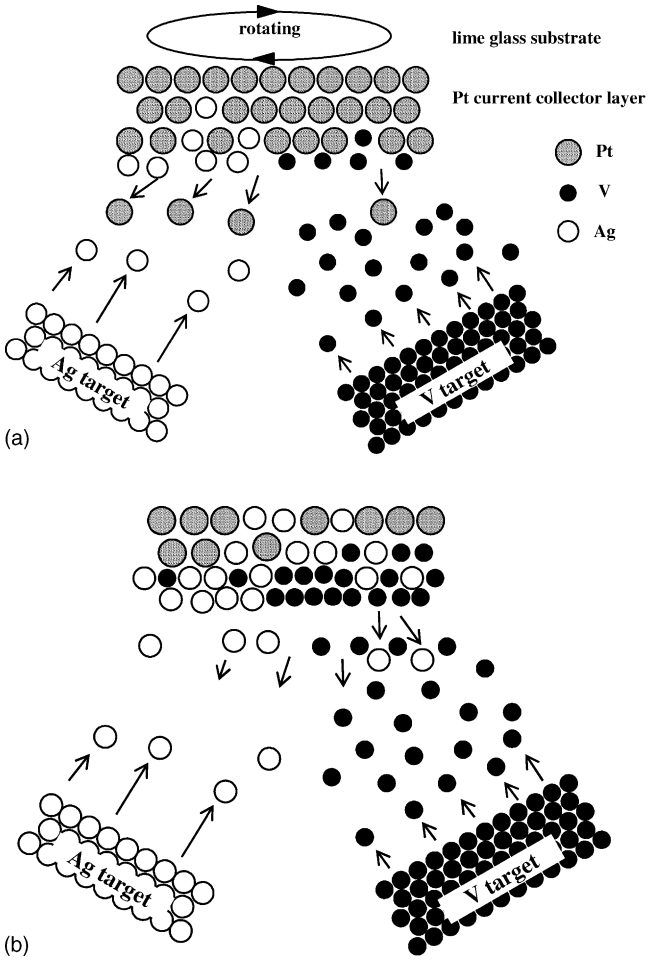

Fig. 12. (a) At initial stage, sputter yield of silver is higher than that of vanadium. Only a small fraction of vanadium is deposited on the platinum layer. A relatively high content of silver atoms is deposited despite of their low flux, (b) on surface of vanadium and silver the sputter yield of vanadium increases more than that of silver. The vanadium deposition rate increases due to high supplied flux.

flux, the sputter yield of each atom usually depends on the mass of each atom [16]. When silver atoms (atomic mass: 107.87) and vanadium atoms (atomic mass: 50.94) sputter simultaneously, the sputter yield of silver is higher than that of vanadium because of its heavier mass. Silver atoms easily adhere to particularly heavy atom substrates (e.g., platinum surfaces) more than vanadium atoms due to less mass difference between source atoms and substrate atoms. The sputter yield of vanadium increases, however, when it is deposited on a lighter material. When vanadium atoms are sputtered on the vanadium surface, they deposit more easily due to less mass difference between source atoms and substrate atoms. During the initial stage of deposition as shown in Fig. 12(a), sputtered vanadium atoms are preferentially re-sputtered owing to the presence of heavy and dense platinum layers. Accordingly, a relatively high quantity of silver is deposited despite the low silver flux. The sputtering yield of vanadium increases after the platinum layer is covered with silver or vanadium. Compared with heavy platinum layers, vanadium atoms adhere more easily on layers composed of silver and vanadium because of the small mass difference as shown in Fig. 12(b). As the coverage of vanadium increases, the sputter yield of vanadium increases.

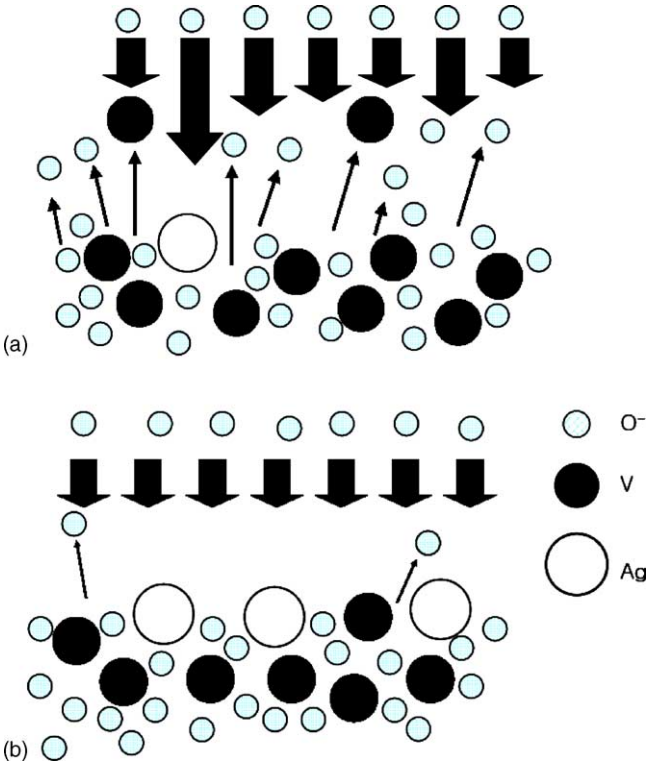

Fig. 13. Different growth mechanisms from (a) low-power condition, (b) high-power condition. Dilute doping of a heavy mass atom results in a sputtering yield amplification effect [5].

4.2. Accelerated pre-sputtering of light elements due to oxygen

During the reactive sputtering process, negative oxygen ions will accelerate towards the growing thin-film. These oxygen ions etch out the layer of thin-film, particularly those composed of light elements, and these by densify the thin-film [5]. On increasing the silver co-sputtering power, the growth rate decreases due to oxygen sputtering on the film that is accelerated by silver atom flux. Under high silver co-sputtering power conditions (A30), however, the silver atoms that stick to the film surface prevent oxygen atoms from etching from the growing thin-film. The case of A40 in particular, due to the high flux of silver the microstructure of thin-film, is different from dense silver vanadium pentoxide. XPS analysis shows a mixture of less oxidized vanadium oxides (e.g., VO_2, V_2O_4, etc.) and metallic silver (Fig. 13).

4.3. Effect of silver co-sputtering on V_2O_5 films

The electrochemical properties of undoped V_2O_5 are improved by silver co-sputtering. According to Smyrl and

co-workers [6–9], dopant silver ($Ag_yV_2O_5$: $y = 0.1$–0.5) enhances the electric conductivity of amorphous-like cathode materials (Xerogel and Aerogel V_2O_5). Due to the increased conductivity, the discharge capacity and cycle ability of the cathode material increases. Lithium-ion diffusivity is found to increase in the silver-doped material with a small dependence on the lithium intercalation level. This is thought to be related to the porosity in this material.

In the present research, the electric properties of vanadium oxide thin-films is increased by the silver co-sputtering process. According to the AES spectra, the silver distribution ion A10 and A20 accumulates at the interface between the platinum current-collector and the V_2O_5 cathode film. In Fig. 6, the capacity increment of A10 during the first cycle is due to the conductivity increase compared with the discharge capacity decay pattern with the undoped sample. It increases during the first cycle and decays with the same pattern as that of the undoped sample (VO).

In sample A30, the discharge capacity during the first cycle and also the 200th cycle increases. This is related to the fact that the 1024 cm^{-1} absorption band of vanadium oxide shifts to 970 cm^{-1} in FT-IR spectra, which means the distance between two adjacent V_2O_5 layers is increased with silver co-sputtering. In XPS analysis, most of the vanadium exists in its well-oxidized state (V^{5+} in V_2O_5) and most silver as AgO and Ag_2O. Considering the FT-IR spectrum, the structure of A30 is silver-doped amorphous V_2O_5 in which the distance between two adjacent layers is widened. Silver distribution increases the conductivity increment and the silver oxide between two vanadium oxide layers increases the diffusivity of lithium ions and the cycle ability.

Notwithstanding the high silver content, the electrochemical properties of the 40 W co-sputtered V_2O_5 thin-film are poor due to the rough and porous structure, as shown in SEM images and AFM images. In the sputtering process, there is preferential deposition on the protruding parts of the rough surfaces because of the easy delivery of sputtered source materials. Most of the cathode surface, except the upper part of cathode clusters, is not covered with solid electrolyte. This electrolyte-free surface is not electrochemically active.

5. Conclusions

The effect of silver co-sputtering on V_2O_5 films has been investigated using GXRD, FT-IR, XPS, AFM, and SEM. It was found that silver co-sputtered samples exhibit better discharge capacity and cycle ability than undoped samples due to a change in microstructure. In particular, a silver 30 W co-sputtered V_2O_5 film exhibits an improved discharge capacity, cycle ability and lithium-ion diffusivity. From FT-IR results it is found that the silver co-sputtering process results in V=O bond elongation due to an increase in the distance between two adjacent V_2O_5 layers. Because lithium ions pass through these layers, the structure change enhances lithium-ion diffusivity and cycle capacity after the 200 cycles. In the case of excess co-sputtering power, e.g., a 40 W co-sputtered sample, a porous structure with defects is observed. This structure degrades the electrochemical properties of the V_2O_5 cathode.

It is concluded that microbatteries using silver-doped amorphous V_2O_5 cathode thin-films are a good choice for microsize power supply systems that may be applicable to smart cards, microsensors and MEMSs actuators.

References

[1] P.B. Koeneman, I.J. Busch-Vishniac, K.L. Wood, J. Microelectromech. Syst. V6 N4 (1997) 355.
[2] N.J. Dudney, J.B. Bates, R.A. Zuhr, S. Young, J.D. Robertson, H.P. Jun, S.A. Hackney, J. Electrochem. Soc. 146 (1999) 2455.
[3] J.B. Bates, N.J. Dudney, D.C. Lubben, G.R. Gruzalski, B.S. Kwak, X. Yu, R.A. Zuhr, J. Power Sources 54 (1995) 58.
[4] L.B. Kublanov, W.J. Bottega, Appl. Math. Modell. 19 (1995) 499.
[5] H.-K. Kim, T.-Y. Seong, Y.S. Yoon, J. Power Sources 112 (2002) 67.
[6] B.B. Owens, S. Passerini, W.H. Smyrl, Electrochim. Acta 45 (1999) 215.
[7] F. Coustier, S. Passerini, W.H. Smyrl, Solid State Ionics 100 (1999) 247.
[8] F. Coustier, J. Hill, B.B. Owens, S. Passerini, W.H. Smyrl, J. Electrochem. Soc. 146 (1999) 1355.
[9] F. Coustier, G. Jarero, S. Passerini, W.H. Smyrl, J. Power Sources 83 (1999) 9.
[10] E. Shembel, R. Apostolova, V. Nagirny, D. Aurbach, B. Markovsky, J. Power Sources 80 (1999) 90.
[11] P. Soudan, J.P. Pereira-Ramos, J. Farcy, G. Gregoire, N. Baffier, Solid State Ionics 135 (2000) 291.
[12] S.V. Pouchko, A.K.I. Schitz, R.G.B. Oooms, J. Schoonman, Solid State Ionics 144 (2001) 151.
[13] M. Benmoussa, E. Ibnouelghazi, A. Bennouna, E.L. Ameziane, Thin Solid Films 265 (1995) 22.
[14] G.B. Hoflund, J.F. Weaver, W.S. Epling, Thin Solid Films 3 (2) (1995) 157.
[15] D. Barreca, G. Andrea Rizzi, E. Tondello, Surf. Sci. Spectra 6 (3) (1999) 168.
[16] S. Berg, I. Katardjiev, Surf. Coat. Technol. 84 (1996) 353.